JOURNAL OF SOLID STATE CHEMISTRY 76, 143–159 (1988)

Time Resolved X-Ray Diffraction of the Thermal Decomposition of $CdCO_3$ Powders Using Synchrotron Radiation

J. R. SCHOONOVER AND S. H. LIN

Department of Chemistry, Arizona State University, Tempe, Arizona 85287-1604

Received December 28, 1987; in revised form April 8, 1988

Time resolved X-ray diffraction (TRXD) is shown to be a viable *in situ* method to quantitatively study solid-state reactions and phase transitions. To demonstrate TRXD, the analysis of time-dependent X-ray diffraction shapes are reported for the isothermal decomposition of $CdCO_3$ powders as a function of temperature. Growth nuclei, stacking faults, disorder, and the influence of temperature during reaction are observed and discussed. Rate laws and activation energies are found for particle growth during reaction and sintering. The formation of CdO from $CdCO_3$ is observed to proceed through several stages from nucleation to the final product.

Introduction

An analysis of the shape of X-ray diffraction line profiles collected by time resolved X-ray diffraction (TRXD) was suggested as an *in situ* method to study the kinetics and mechanism of solid-state reactions and phase transitions (*1*). TRXD provides quantitative global information for systems in which the environment is carefully controlled and is therefore complementary to microscopy. Control of the reaction environment, in particular the partial pressure, may be used to study one or more reversible reaction mechanism steps. For example, CO_2 pressure affects carbonate decomposition kinetics (*17*), and H_2O pressure may influence Ostwald ripening (*12*). In this way, TRXD will fill an important role in solid state chemistry.

A brief examination of the thermal decomposition of $Cd(OH)_2$ powders showed the feasibility of the method (*2*). In this paper, to further demonstrate the capabilities of TRXD, the TRXD of the formation of cubic CdO from hexagonal $CdCO_3$ in air is reported.

Solid-state reactions of this type, i.e., decomposition reactions of hydroxides, carbonates, etc., are of the utmost importance in the preparation of ceramics and catalysts. The properties of these materials depend not just upon the chemical composition, but also on the specimen history. Thus an understanding of the kinetics and mechanism of decomposition reactions is important in the application of these materials (*3*). Cadmium carbonate is considered in this work because its diffraction pattern and kinetics are amendable to an introductory TRXD study.

Synchrotron radiation at a Stanford Synchrotron Radiation Laboratory (SSRL) wiggler line was used as the X-ray source.

0022-4596/88 $3.00

The advantages of using synchrotron radiation over conventional sources arise from its high intensity and collimation (i.e., high brilliance) and the near Gaussian energy distribution of the beam after its passage through the monochromater. The high intensity improves time resolution in an obvious manner; the high collimation reduces flat specimen, specimen transparency, and divergence aberrations; the energy distribution avoids distortion by undesired components and reduces the extent of the tails, hence decreasing profile overlap, width of the scan region, and collection time. Angular resolution may be sacrificed for time resolution by removing the söller slits and analyzer from the diffracted beam path. By this means profiles with time and angular resolutions that are not possible to achieve with other sources, such as a rotating anode, are obtained.

Experimental

The TRXD lines for the isothermal decomposition of $CdCO_3$ powders were collected at SSRL at an eight pole wiggler side station with an unfocused Si (220) monochrometer tuned at 8.0 keV. A germanium detector was step scanned at $2\theta = 0.030°$ intervals with a 1- to 2-sec dwell and a 0.33-sec wait between steps to allow for vibrational dampening of the detector arm. To improve time resolution, söller slits and an analyzer were removed from the beam path.

CdO profiles were collected *in situ* during the isothermal decomposition at $CdCO_3$ in air as a function of time for temperatures from 649 to 700 K. $CdCO_3$ profiles were often scanned simultaneously to serve as monitors.

The $CdCO_3$ powders were prepared by Brauer's method (*4*). Each set of experiments was performed with the same preparation.

The instrument profiles were measured using a sample of CdO annealed at 775 K for 36 hr. The profiles were step scanned with 2θ intervals of 0.010° with a 5-sec dwell.

Isothermogravimetry was performed with a Cahn 1000 electrobalance. The furnace was external to the hangdown tube and a Chromal–Alumal thermocouple was positioned just below the sample bucket. Each sample was approximately 100 mg and was spread evenly and loosely with a maximum thickness of 1 mm for a uniform thermal distribution.

Data Analysis

The data were analyzed for size and strain using the variance-range method (*5–7*). In this method the variance as a function of the range of integration, $W(\sigma)$, is fitted to the linear equation

$$W(\sigma) = k\sigma + W_0. \quad (1)$$

The particle size, p, is given by

$$k = \frac{\lambda K_w}{2\pi^2 p \cos\theta}, \quad (2)$$

where λ is the wavelength and K_w is the Scherrer constant for the variance. The variance of the strain, $\langle e^2 \rangle$, is given by

$$W_0 = -\frac{\lambda^2 L}{4\pi^2 p^2 \cos\theta} + \langle e^2 \rangle \tan^2\theta, \quad (3)$$

where L is the taper parameter.

Because of profile overlap and the large signal-to-noise ratio in the extremities of the tails, the truncated variance (*6*),

$$W_2(\sigma) = \frac{\int_{-\sigma}^{+\sigma} (2\theta - \langle 2\theta \rangle)^2 I(2\theta) d(2\theta)}{\int_{-\sigma}^{+\sigma} I(2\theta) d(2\theta)}, \quad (4)$$

was used in Eq. (1); here, $\langle 2\theta \rangle$ is the centroid of the profile with intensity I at position 2θ. Since the profiles were symmetric throughout most of the reaction, the integration limits, σ, could be taken as symmet-

ric. Equation (4) is valid as long as the truncation is never more than 15% (*6*).

The profile background, the range of integration for Eqs. (4) and (1), and the fit to Eq. (1) were determined simultaneously using the iterative method of Langford and Wilson (*8*); the background was taken as linear and deconvoluted by subtraction. The initial background used was that for the unreacted specimen.

The variance for the instrument profile was deconvoluted using the additivity property of the variance.

No profile refinement was performed, although profiles collected early in the reaction were smoothed with a variable knot cubic splines algorithm after the background was removed by subtraction. For profiles collected later, smoothing gave no advantage and indeed often distorted the data by not always giving good treatment in the region of the mode.

Errors in the slope and intercept caused by the truncation of the profiles and the nonadditivity of the components of the experimental profile were corrected for in the manner of Langford (*6*). The truncation errors in k (Δk) and in W_0 (ΔW_0) were corrected for by subtracting the relations

$$\Delta k \simeq k_2^2,$$
$$\Delta W_0 \simeq -W_{02}/\langle\sigma\rangle^2, \qquad (5)$$

from the respective values. The nonadditivity error was corrected for by adding to the right side of Eq. (1)

$$W_{na} = -1/2\pi^2 k_g k_f, \qquad (6)$$

where k_g is the slope of the variance-range function for the specimen profile and k_f is that for the instrument profile (*6*). Since the effects of the nonlinear terms in the variance-range equation are usually negligible, no curvature correction was performed.

For many data collections, to improve the time resolution, the 2θ range was reduced and hence was not sufficient to use the variance-range equation with confidence. For such cases, if strain broadening is assumed to be negligible, and the particle shape spherical (so that the taper parameter is zero), Eq. (2) reduces to

$$W = \frac{\lambda K_w}{2\pi^2 p \cos\theta}, \qquad (7)$$

from which the particle size may be found directly from the variance. For convenience, when this equation is used to determine the particle size, it will be referred to as the variance-breadth method, rather than the variance-range method for which Eq. (1) is used.

The CdO profiles were analyzed for spherical and cubic crystallites. The shape of the oxide particles were approximated as cubic, but spherical shapes were also considered for comparison of the variance-range results with those from the variance-breadth.

Results

Isothermogravimetry. The kinetics of CO_2 loss during the isothermal decomposition are first order for an extent of the reaction (α) between 0.1 and 0.7 to 0.8. Nonisothermal heating in the first part of the curves accounts for the deviation from first-order kinetics up to $\alpha = \sim 0.1$. An Arrhenius plot gives an activation energy of 107 kJ/mole (Table I), which is comparable to the literature values (*9*, *10*). The lowest

TABLE I

ACTIVATION ENERGIES AND PREEXPONENTIAL FACTORS FOR THE RATE CONSTANTS FOR CdO GROWTH

	Activation energy (kJ/mole)	Preexponential factor (sec^{-1})
Reaction	155.3	2.34×10^9
Sintering	154.9	2.66×10^{10}
Isothermal analysis	107	4.56×10^3

TABLE II

LINES OBSERVED FOR THE UNIDENTIFIED RADIATION PRODUCED PHASES IN $CdCO_3$ POWDER

Position (deg)	I/I_0	d-Spacing (Å)
33.99	33	2.72
41.41	45	2.25
66.10	9	1.46
66.82	8	1.44
68.02	100	1.42
71.63	57	1.36

temperature scans, those with a "sluggish behavior," did not fit the Arrhenius plot, the rate constants tending to be too low.

The instrument profiles. The instrument profiles are asymmetric, the low-angle tails having a greater intensity than the high-angle tails. This asymmetry is consistent with what is expected from flat specimen, specimen transparency, and divergence aberrations, and is a general feature of synchrotron radiation powder X-ray diffraction (*11*). The full width at half the maximum intensity (FWHM) is ~0.12° for all line profiles and is constant with 2θ.

The radiation produced phase profiles. For the $CdCO_3$ samples used in this TRXD investigation, radiation damage was observed. It appeared as a brown image on the specimen face. The peak positions and the relative intensities of the radiation produced phase (RPP) are presented in Table II. The lines are sharp and have a low intensity, usually less than 1% of the carbonate lines. Their FWHM is approximately that of the instrument profiles, and they display the same asymmetry. Regardless of the length of time of irradiation, the intensity of the lines remain constant, indicating that only a small fraction of small- and/or high-defect $CdCO_3$ crystallites are involved. Upon application of heat the lines decrease in intensity as the phase reacts to form the oxide (there is no evidence from X-ray diffraction that it forms still another phase upon reaction). Quantitative time-dependent information of these lines is not reliable, since they are of low intensity and those observed usually suffer overlap with oxide lines. This overlap occurs with the CdO (111) and the CdO (311), so that these lines are not considered in detail. A deconvolution has been performed, but because the noise level is high, the results are not considered here.

The full width at half the maximum intensity. Examples of the TRXD profiles are presented in Fig. 1. The FWHM of the carbonate and the RPP line profiles decrease with reaction time. As the reaction proceeds, the FWHM of the carbonate profile decreases and approaches that of the instrument profile, at which the widths become erratic as the profiles dissolve into the background. The RPP line profiles behave similarly. This behavior is ascribed to specimen broadening.

The FWHM for the CdO (200) and (220) profiles decrease with reaction, the rate of which increases with temperature. After reaction, the FWHM still decreases, but at a smaller and constant rate.

Asymmetry of the oxide line profiles. The first few scans of the CdO (200) and CdO (220) lines, and their higher orders, are asymmetric in a manner opposite to that expected from instrument aberrations: the tails are more extensive for the high 2θ side than for the low (e.g., Fig. 2). There is no asymmetry for the CdO (111) or (222) profiles. The magnitude of the asymmetry for the data analyzed is usually a one to two step scan (0.030 to 0.060°) difference in the positions of the FWHM profile tie lines as measured from the mode. This asymmetry decreases with reaction. At an extent of reaction less than 0.3 the profiles become symmetric and remain so throughout the remainder of the reaction; the asymmetric instrument profile is buried by the broad specimen profile.

The $CdCO_3$ and the RPP line profiles show the same asymmetry as the instru-

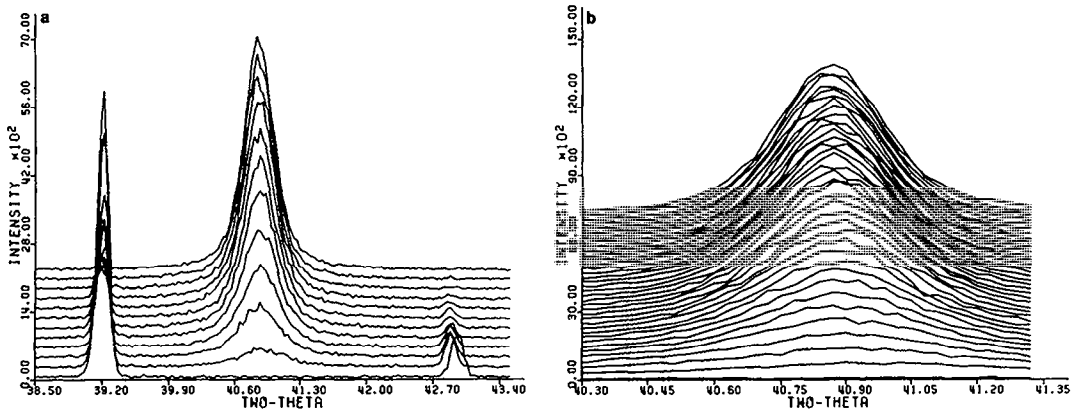

FIG. 1. The TRXD profiles for CdO (200). The lowermost profile is for zero reaction time. The profiles have not been smoothed. (a) The profiles at a decomposition temperature of 655 K. The profiles at $2\theta = 39.2$ are $CdCO_3$ (110), at 40.8 are CdO (200), and at 42.9 are of the RPP. Each scan is at every ~4.4 min, the lowest for zero time. (b) The profiles at a decomposition temperature of 675 K. Each scan is at every ~1 min.

ment profiles throughout the reaction; therefore, the CdO profiles asymmetry is of the specimen profiles.

It must be noted that the asymmetry occurs when the rate of reaction is the greatest and decreases as the rate decreases. For fixed energy scanning TRXD, as the diffraction line is scanned from low to high angle, the number and size of diffraction domains increase with time. This increases the intensity of the line profile as it is scanned and may conceivably produce an asymmetry on the high-angle side. However, for a first-order reaction for phases with Gaussian and Lorentzian profile functions, the width of the line decreases and the mode is shifted, but in such a manner that there is no change in the symmetry of the profile. This situation is a good approximation to the TRXD experiments performed and suggests that the distortion by step scanning is insignificant. Thus, even with consideration of the method of data collection, the conclusion remains that the line profile asymmetry is of the specimen.

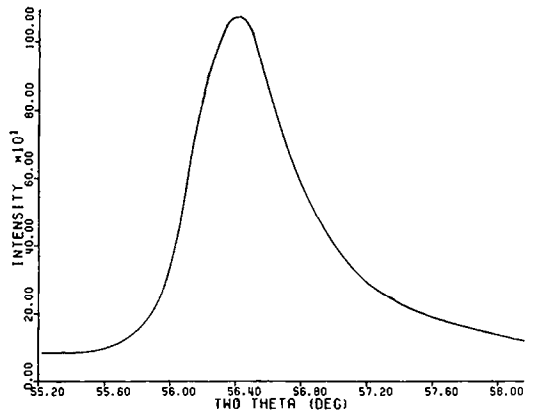

FIG. 2. A smoothed TRXD profile for CdO (220) at a high temperature (approximately 715 K) showing the asymmetry of the profiles just after the reaction began.

The position of the oxide line profiles. With reaction the CdO peak position shifts to higher 2θ. This is opposite to what is expected from thermal expansion, and suggests that there is a strain in the solid such that the average Cd^{2+} spacing is less than that for the final oxide product. The shift is usually about one step scan, 0.030°, but tends to be the largest for the first few scans of the reaction and may be related to the asymmetry. After reaction, the peak position remains constant.

The CdO (111) integrated intensities. If

the RPP lines that are convoluted with the oxide lines are asummed to decay with the same kinetics as the carbonate and the RPP lines that are free from overlap, then their integrated intensity at a given time may be predicted. From this the integrated intensity of the oxide profiles that are convoluted with the RPP profiles may be approximated by subtraction from the convoluted profile integrated intensity. The extent of reaction, α, may then be found for the oxide profile suffering overlap using the integrated intensity of the fully reacted specimen (i.e., $A(t)/A(\infty) = \alpha$, where $A(t)$ is the integrated intensity at time t). Alternatively, the oxide profile intensity at a given time may be predicted from the kinetics of the oxide profiles free from overlap, from which the integrated intensity of the RPP line may be found by subtraction. The fraction of the specimen reacted, β, may then be found using the integrated intensity of the RPP line before reaction. If both convoluted lines follow kinetics that are identical to that of the other profiles, then $\alpha + \beta = 1$. For the CdO (311) profile this is found to hold within ±5%, but for the CdO (111) it is ~30% too large for the first few minutes of the reaction. Either the CdO (111) or the overlapping RPP line does not follow the same kinetics as the other profiles. Upon comparison of the data for all other profiles, it appears that the CdO (111) profiles do indeed grow in faster than expected. Thus, the initial integrated intensities of the CdO (111) profiles are disproportionately large.

Particle sizes by the variance-breadth method for the CdO (220) and (220) reflections. The particle sizes as a function of time from the variance-breadth are presented in Fig. 3 and the integrated intensities for each in Fig. 4. For the CdO (200) and CdO (220), the size as a function of time displays two distinct time regimes. The first time regime corresponds to growth during reaction (when the integrated intensity is increasing with time); however, at 700 K this regime extends beyond $\alpha = 1$. The second regime begins after decomposition has completed, but has not been studied to the time when the experimental profile FWHM approaches that of the instrumental. In this regime growth is by sintering without reaction. These two regimes are separated by a discontinuity in the kinetics; when strain is removed, the discontinuity appears as an inflection in the growth curves. The rate of growth for both regimes increases with temperature.

For CdO (220), the "initial" sizes (sizes within the first ~30 sec of the reaction as measured directly or extrapolated to 30 sec)

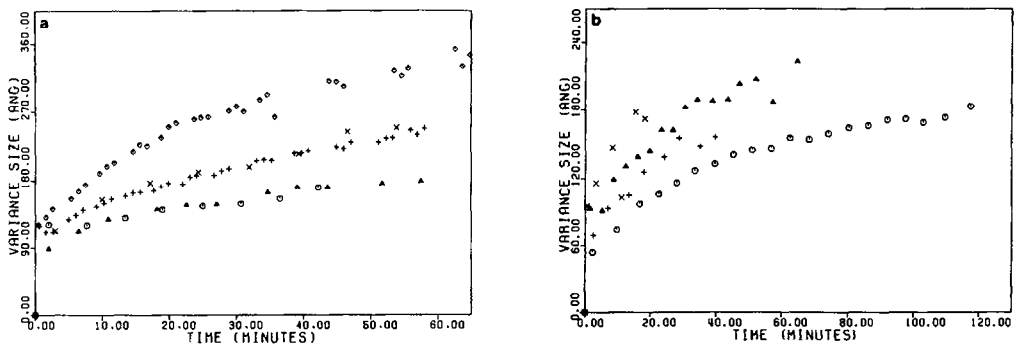

FIG. 3. The particle sizes from the variance as a function of time for various temperatures. (a) The variance for the CdO (200) planes. The temperatures are 649 K, ○; 655 K, △; 675 K, +; 675 K, sample II, X; 700 K, ◇. (b) The variance for the CdO (220) planes. The temperatures are 649 K, ○; 675 K, △; 675 K, sample II, +; 700 K, X.

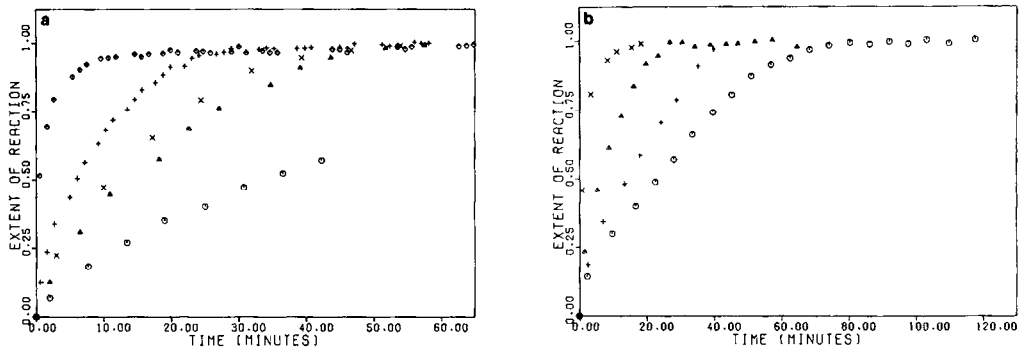

FIG. 4. The extent of the reaction as a function of time as measured by the TRXD integrated intensities for various temperatures. (a) The extent of the reaction for the CdO (200) plane. The temperatures are 649 K, ○; 655 K, △; 675 K, +; 675 K, sample II, X; 700 K, ◇. (b) The extent of the reaction for the CdO (220) plane. The temperatures are 649 K, ○; 675 K, △; 675 K, sample II, +; 700 K, X.

range from ~50 Å to 649 K to ~95 Å at 700 K. The sizes near the inflection for the CdO (220) reflections are ~145 Å for temperatures below 700 K, but at 700 K the size is larger, being ~170 Å.

A similar trend is seen for the CdO (200) reflections. The initial size increases with temperature from ~90 Å at 649 K to 130 Å at 700 K. The final particle size is ~170 Å, for temperatures below 700 K; the sizes may increase with temperature, but this is uncertain, since the apparent change is only 6 Å from 655 to 675 K. At 700 K the final size is much larger than for lower temperatures, being ~225 Å.

For both planes, the particle size after decomposition is complete increases with temperature.

There is a sample dependence. The better crystallized samples result in larger product particle sizes, although the initial sizes are comparable for both samples studied.

In summary, for both planes, for the assumption of spherical particles, the initial particle size increases with temperature, but the final product for temperatures below 700 K is constant with temperature. At 700 K, the size is substantially larger. The results for the final sizes are in agreement with the investigation of Munir and Asirvatham (*12*) for static X-ray measurements.

The kinetics of particle growth from the CdO (200) and CdO (220) reflections. The results imply that the kinetics of growth of the oxide are temperature dependent and may be divided into two regions. The first region is associated with reaction and the second with postreaction annealing and sintering.

For the CdO (220) and (200) reflections growth during reaction is a first-order process described by

$$S(t) = S_0[1 - S_c \exp(-kt)], \qquad (8)$$

where k is the first-order rate constant, $S(t)$ is the particle size at time t, S_0 is the average particle size at the end of reaction, and S_c is a constant that depends on the critical size. The results of a linear least-squares fit of Eq. (8) are presented in Table III for CdO (220) and CdO (200). The final particle sizes are determined empirically. An Arrhenius plot (Fig. 5) gives for the rate constant for both planes

$$k = 2.3 \times 10^9 \text{ sec}^{-1} \exp\left[-\frac{155.3 \times 10^3 \text{ J/mole}}{RT}\right]. \qquad (9)$$

TABLE III

FIRST-ORDER RATE CONSTANTS FOUND BY THE VARIANCE-BREADTH METHOD FOR THE FORMATION OF CdO FROM THE DECOMPOSITION OF $CdCO_3$

(*hkl*)	Temperature (K)	k (min^{-1})	S_c	S_0 (Å)
(220)	649	0.044	0.72	146
(220)[a]	649	0.047	0.98	160
(220)	675	0.094	0.46	145
(200)	655	0.059	0.51	171
(200)	675	0.139	0.57	177
(200)	700	0.226	0.83	226
(200)[b]	675	0.064	0.54	215

[a] Above the inflection region.
[b] Sample II.

At 700 K, the data do not follow the linear Arrhenius relation, implying a lower activation energy, preexponential factor, or both. The above results are for the assumption that the plot is linear below 700 K.

Postreaction annealing and sintering is a zero-order process over the time observed; the size at time t is given by

$$S(t) = kt + C, \qquad (10)$$

where k is the zero-order rate constant, C is a constant, and $S(t)$ is the average size at time t. The rate constants and the constants C were found by linear least-squares for the experiments of long temporal duration and are presented in Table IV for various temperatures for the CdO (111), (200), and (220) reflections. The Arrhenius plot (Fig. 6) gives for the rate constant for all planes measured at 675 K or lower (Table I)

$$k = 2.7 \times 10^{10}\ \text{sec}^{-1} \exp\left[-\frac{154.9 \times 10^3\ \text{J/mole}}{RT}\right]. \qquad (11)$$

Sintering and annealing are kinetically isotropic, and the rate constant differs from that during reaction only by the preexponential term. Again, at 700 K the rate constant has a lower value than expected from the Arrhenius plot; the average deviation of these latter data points from the expected linear curve, as extrapolated from below 700 K, are the same for both Arrhenius plots, both being about 0.60.

The behavior of the data at 700 K for both Arrhenius plots is similar to the iso-

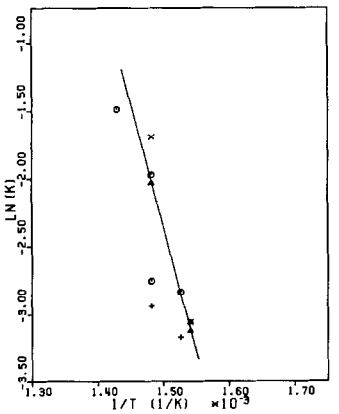

FIG. 5. The Arrhenius plot for the first-order rate constant for the kinetics of growth by reaction for several planes as measured by the variance. The planes are CdO (220), △; CdO (200), ○. The kinetics as measured by the variance-range method are also plotted. The planes are CdO (220), X; CdO (200), +.

TABLE IV

ZERO-ORDER RATE CONSTANTS FOUND BY THE VARIANCE-BREADTH METHOD FOR THE SINTERING OF CdO FROM THE DECOMPOSITION OF $CdCO_3$

(*hkl*)	Temperature (K)	k (min^{-1})	C (Å/min)
(220)[a]	649	0.057	115.366
(220)[a]	675	1.616	123.616
(220)	700	2.940	122.477
(200)[a]	655	0.601	145.232
(200)[a]	675	1.717	146.724
(200)	700	2.083	210.867
(111)[a]	662	1.113	137.328
(111)[a]	675	1.558	174.346
(111)	675	3.103	56.087
(111)	700	3.20	220.268

[a] Data points used in the Arrhenius plot least-squares fit.

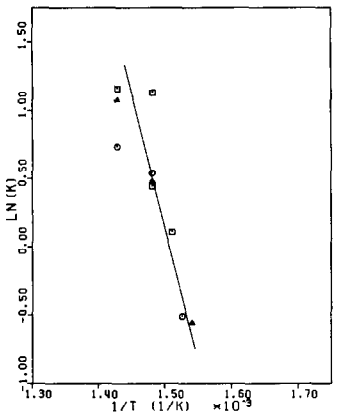

FIG. 6. The Arrhenius plot for the zero-order rate constant for the kinetics of growth by sintering for several planes as measured by the variance. The planes are CdO (111), □; CdO (220), △; CdO (200), ○.

thermal TGA results of Mikhail *et al.* (*13*) for doped samples and of Asirvatham and Munir (*10*) for pure samples.

Size and strain from the CdO (200) and CdO (220) reflections from the variance-range method. The variance-range method shows that both size and strain contribute to the specimen line broadening. As for the results for the variance-breadth method, the time-dependent results for the variance-range method may be divided into two parts: a part associated with the reaction and a part associated with only annealing and sintering of the final product phase. The end of the reaction as determined by the size and strain distributions from the variance-range method corresponds to the end of the reaction as determined by the integrated intensities and the size distribution from the variance-breadth method.

Strain makes its largest contribution during reaction and decreases with reaction time, after which it becomes nearly constant, only slowly approaching zero, but never becoming zero (Fig. 7). Qualitatively, the kinetics of annealing during reaction increases with temperature, but a kinetics equation for strain annealing during the reaction period could not be determined. The rate of annealing during reaction appears to be the same for both reflections, although the (200) reflection may show a greater amount of strain. There are no appreciable differences in the behavior of the strain between different samples. After reaction, the annealing kinetics are best described as a zero-order process with a rate constant near zero. The temperature dependence of the strain in the oxide crystallites is such that with decreasing reaction time, the initially measured strain increases. After reaction, there is no obvious relationship between the values of the strain determined from different temperatures.

An interesting observation is that the variance of the strain is negative for the assumptions of cubic and spherical crystallites. This is consistent with the shift in the mode at the end of the reaction. This shift suggests a negative strain in the product during reaction. If the strain distribution has a maximum at a lattice spacing that is less than that for the end product oxide, or is asymmetric with respect to negative strain, then the variance would be expected to be negative. This may be seen more clearly through the expression for the variance:

$$\langle e \rangle = \int (x_0 - x)^2 f(x_0 - x) dx,$$

where $\langle e \rangle$ is the strain, x_0 the position of a Cd^{2+} in the final oxide product, x the position of Cd^{2+} during reaction when there is strain present, and $f(x_0 - x)$ is the strain distribution function.

Qualitatively, the behavior of the variance of the strain and particle size are the same for both assumptions of cubic and spherical shapes.

The time dependence of the average size has an unusual behavior (Fig. 8). This is seen particularly well for the (220) reflection. The average size asymptotically approaches a maximum value just before the end of the reaction; the average size re-

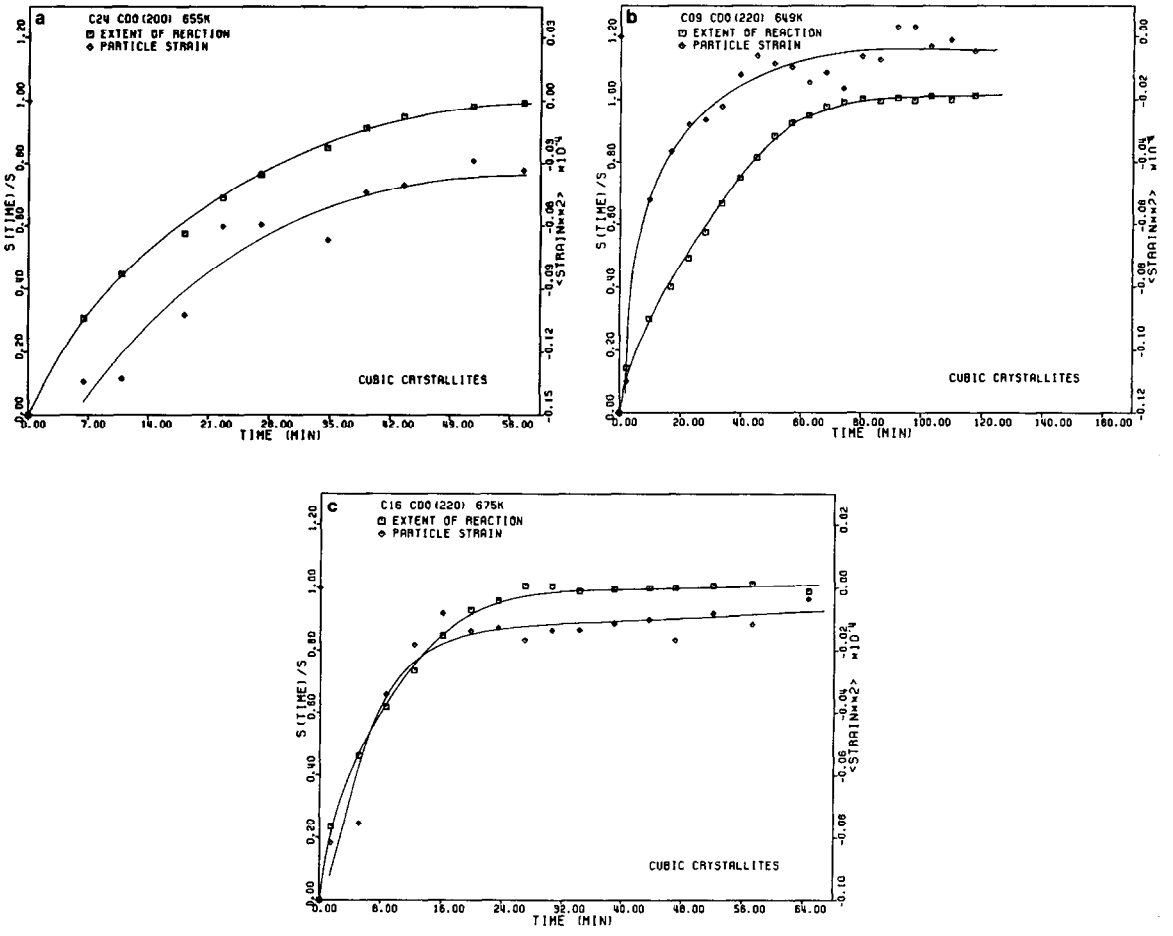

FIG. 7. The variance of the strain along with the extent of the reaction as measured from the integrated intensity as a function of time. (a) The variance of the strain for the CdO (200) plane at 655 K. (b) The variance of the strain for the CdO (220) plane at 649 K. (c) The variance of the strain for the CdO (220) plane at 675 K.

mains at the asymptotic value until reaction is completely over, after which a resurgence of growth occurs. Finally, the rate of growth levels off and the average size remains on a plateau. Thus, an inflection is seen in the curve.

The inflections correspond to the discontinuities in the size distribution as a function time from the variance-breadth and the FWHM. For the CdO (220) reflection, the inflection occurs between an extent of the reaction from 0.9 at 649 K to 0.7 at 675 K; for the CdO (200) reflection, this inflection is not nearly as severe and does not occur until nearly the end of the decomposition, and for a second, better crystallized sample, the inflection is not seen at all (Table I). It is notable that this inflection occurs at approximately the same extent of the reaction as when a first-order plot for isothermalgravimetry is no longer valid.

For the assumption of spherical particles, within the time resolution of the experiment, the CdO (220) reflection measure-

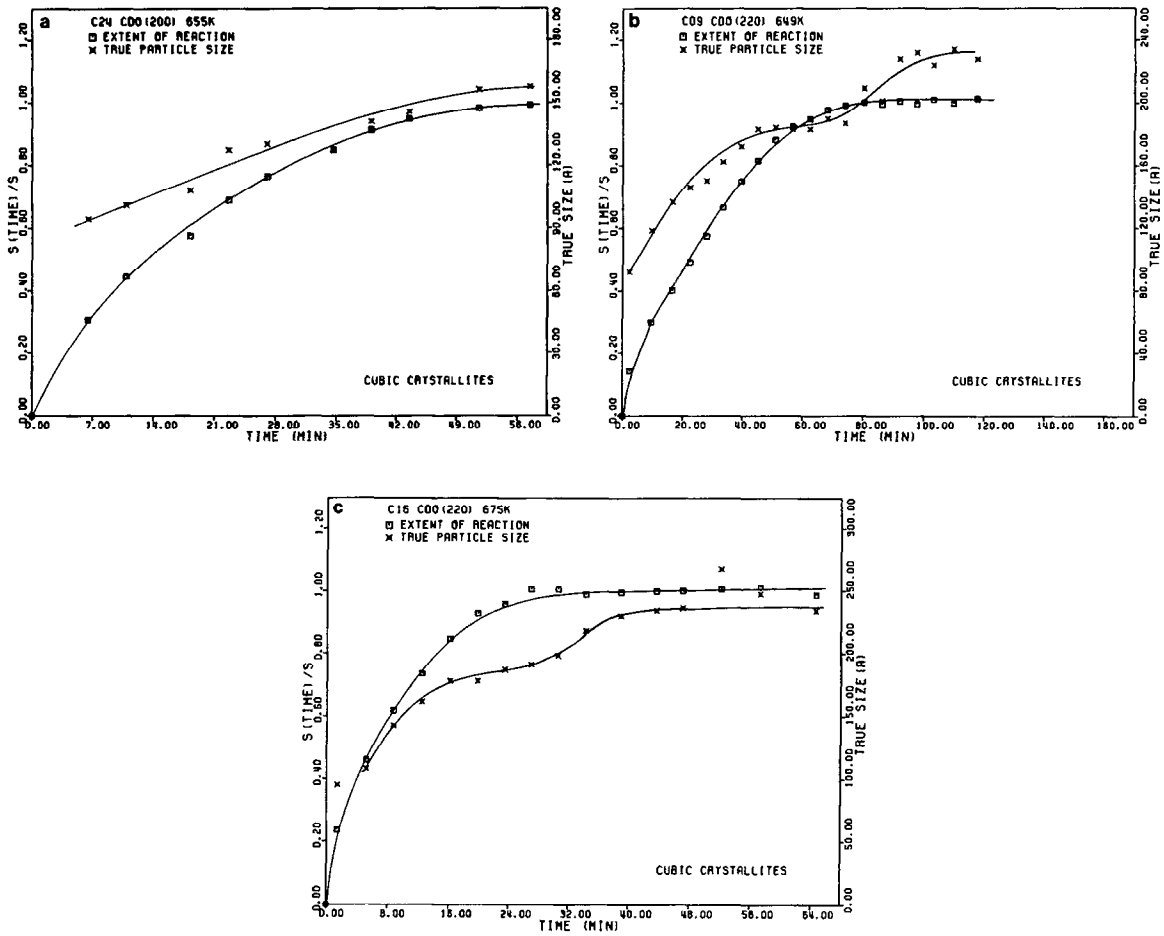

FIG. 8. The size of the particle along with the integrated intensity as a function of time as determined by the variance-range method. (a) The size of the particles from the CdO (200) plane at 655 K. (b) The size of the particles for CdO (220) plane at 649 K. (c) The size of the particles for CdO (220) plane at 675 K.

ments show the same average particle size at both temperatures measured for the same sample at the beginning of the experiment (~90 Å) and at the inflection (~160 Å), although for the experiment at 675 K, the inflection is at a lower extent of the reaction since the rate is greater. The final particle size is temperature dependent (~200 Å at 649 K and ~220 Å at 675 K).

The CdO (200) reflection measurements give similar particle sizes to the CdO (220) measurements at the beginning of the observations (~100 Å or larger) and at the inflection (~160 Å); at the end of the reaction the size is ~190 Å. A second, better crystallized sample behaves similarly, but the average sizes are larger.

The kinetics of growth for the first stage are first order for both reflections. The rate constants determined by linear least-squares for Eq. (4) are presented in Table V. Likewise, the kinetics for growth above the inflection is also first order, but a determination of the rate constant was only pos-

TABLE V

FIRST-ORDER RATE CONSTANTS FOUND BY THE VARIANCE-RANGE METHOD FOR THE FORMATION OF CdO FROM THE DECOMPOSITION OF $CdCO_3$

(*hkl*)	Temperature (K)	k (min^{-1})	S_c	S_0 (Å)
(220)	649	0.047	0.55	180
(220)	675	0.184	1.03	180
(200)	655	0.042	0.58	160
(200)[a]	675	0.053	0.36	180

[a] Sample II.

sible for one experiment, the CdO (220) reflection at 649 K; there is an insufficient number of data points for the other curves to justify a determination.

The rate constants are plotted on the same Arrhenius plot as for the variance-breadth method (Fig. 8). These data points fall close to the line for the results from the variance-breadth method, but with a larger scatter. A new curve through them may result in a slightly larger activation energy, but given the small number of data points this is not presented.

Discussion

Comparison of the particle sizes from the variance-range and the variance-breadth methods. It is expected upon application of the variance-range method with the assumption of spherical particles that with the removal of strain broadening the measured particle size should be greater than that for the variance-breadth method if disorder is significant during the reaction. When the decomposition is over or near completion, the two treatments should give similar results if the strain approaches zero.

This is observed. For the CdO (200) data sets, for the first scans during reaction, with the removal of disorder, there is a 20% increase in size at 655 K and 40% increase in size at 675 K. For both experiments, near the end of reaction, the particle sizes determined by the two methods approach within a few percentage of one another. At the inflection, the particle sizes are within 6% of one another, and the strain broadening may be somewhat larger than that after decomposition has gone to completion.

For the CdO (220) experiments at 649 and 675 K, for which data collection extends well beyond the end of the reaction, the results are similar. The particle sizes measured early in the reaction are larger by ~10%; the sizes in the region of the reflection differ by about the same as those at the end of the reaction and show no substantial strain. Again the separation of the strain implies larger particle sizes.

A comparison of the particle sizes from the two methods and the strain measurements indicate that there is only a small amount of strain broadening at the end of reaction, and subsequent changes in line shape are primarily a size effect.

At the inflections, there is still some disorder present. The loss of disorder at this time concludes the growth during reaction and precedes the growth by sintering; i.e., the kinetics at this point are changing from first order to zero order.

In contrast, there is a substantial strain broadening during reaction. An obvious difference between the results of the two methods is that the initial particle size from the variance-breadth is temperature dependent. This dependence is opposite to what is expected if the strain observed is that of the reaction itself; the decrease in strain with temperature therefore is annealing of disorder in the initial product formed by reaction.

Neglecting strain results in too large rate constants for particle growth during reaction for the temperature range investigated. This results in a slightly lower activation energy, but the value should not differ substantially from that found otherwise.

Growth nuclei. Three characteristics of

the CdO growth in the early part of the reaction stand out. The first is the large initial particle size. It is seen that at 10 to 20% decomposition, the particle sizes are 50 to 60% of the final size. A more detailed consideration shows that the size increases with the square root of the volume fraction of CdO (*14*); with this accounted for, and the curves extrapolated to zero time, the particle sizes are 2.5 to 3.5 times too large. This large initial size is not consistent with the observed kinetics unless a constant is included in the rate law. The second feature is the large amount of disorder during reaction. This is seen in particular for the first few minutes of the reaction by the profile asymmetry. The third prominent feature is the disproportionately large CdO (111) integrated line intensity early in the reaction. This integrated intensity may be as much as 30% larger than what is expected from other profiles.

There are two obvious ways to explain the large initial particle size. The first is that the product particles form rapidly, and that the growth observed during reaction is actually from a change in the particle size distribution as a result of sintering rather than reaction. However, it is seen that the growth during reaction is associated with the reaction. The variance range curves show an abrupt change in overall shape at the end of reaction, and the temporal behavior of the strain shows that a rearrangement of atoms is occurring during reaction. Also, both the FWHM and the variance-breadth show marked differences in behavior before and after reaction. The activation energies do show that growth during and after reaction are related, as is discussed below, but there are also differences as seen in the preexponential factor.

A second explanation is that the large initial size represents a growth nucleus. This size is larger than what is expected for a growth nucleus, but it must be recalled that the growth nucleus for phase transitions may be quite large; for example, in zirconia the growth nucleus may be several hundred angstroms (*15*).

The second prominent feature, the disorder during the reaction, suggests, as mentioned above, a rearrangement occurring during the reaction. The disorder manifested as strain no doubt arises from the rearrangement of atoms at the topotactic planes. The amount of rearrangement may be different for different planes, as is demonstrated by removing disorder broadening from the profile breadth. In addition, rearrangement may be occurring on a much broader scale, as shown by the asymmetry of the diffraction profiles collected at small time.

Arguments that the asymmetry is not the result of the arrangement of the experiment were presented earlier. The observed asymmetry of the oxide profiles during reaction is often associated with twin faults and stacking faults (*5, 16*). These mistakes are expected to give asymmetric profiles for both the (200) and the (220) profiles, but not for the CdO (111) line profile; if a CdO (111) line profile can be obtained free from overlap, the absence or presence of asymmetry would help confirm any conclusions drawn concerning mistakes during the reaction. The loss of the remarkable asymmetry for the scorched specimen (Fig. 2) indicates that with reaction the mistakes are annealed from the specimen; however, this apparent decrease in asymmetry is caused by a change in the relative contribution of each of the profiles for mistake, size, and strain distribution to the total specimen profile. As the reaction proceeds, the smaller fraction of crystallites with mistakes makes a smaller contribution to the total profile. The loss of asymmetry does not indicate that stacking mistakes are no longer forming, or entirely annealed out, but rather their influence on the total profile is less. What is evident is that since the origin of the asymmetry has its greatest ef-

fect early in the reaction, before the size distribution is dominated by large particles and when the strain is the greatest, it is associated with the earliest stages of the reaction. If stacking mistakes are indeed present, then they must be part of the earliest stages of crystallographic conversion. The layers of atoms then rearrange themselves into the final oxide product.

Finally, the third prominent feature is the apparently large integrated intensity for the CdO (111) lines early in the reaction. There are two possible causes for this. The first is a preferred orientation of the oxide particles, for which the (111) planes are parallel to the specimen face. The second possibility is that disorder leads to a low diffraction power of other planes.

The first possibility requires that the preferred orientation of the product phase be lost with reaction as the carbonate diffraction domains are broken up. This also may imply a preferred orientation of the reactant, so that the preferred orientation of each phase would lead to a conclusion about the topotaxy. The carbonate powder diffraction patterns show no preferred orientation; however, observations during specimen packing indicate that there is a preferred orientation favoring [001] if the sample is not properly ground; this preferred orientation would not be readily apparent in the diffraction pattern as the (001) reflections are too weak (only the reflection for $l = 6$, which is of very low intensity, has been observed). Finally, the diffraction pattern of the oxide at the end of reaction does not show relative intensities that correspond to that of random orientation; indeed, the CdO (111) reflection intensity is somewhat lower than expected, and the CdO (200) and the CdO (220) reflection intensities are larger than expected. This anomaly in intensities cannot be explained by a shifting of intensity into the tails of the CdO (111) line at the expense of the body of the line, as the FWHM at the end of the reaction is not substantially different between line profiles (which is just what is expected from the particle size determination and the instrument profiles). In conclusion, if the large initial integrated intensity is indeed the case, and if it is caused by a preferred orientation, then that preferred orientation corresponds with the $CdCO_3$ [001] and is lost during the progress of the reaction.

The second possibility, the one that is preferred over the former by the above arguments, is supported by the presence of stacking mistakes. The disorder decreases the integrated intensity of the other profiles and suggests that the extent of reaction is much larger than is observed by them. The formation of the growth nucleus cannot be by the addition of complete unit cells. To see this, consider the addition of a perfect unit cell onto a diffraction domain of any size or shape. The addition of this unit cell would increase the size of all planes proportionately, and hence would have a corresponding effect on the diffraction power of all planes. The behavior cannot be due to growth alone. This suggests that the formation of the growth nucleus is by rearrangement of the topotactic $CdCO_3$ planes after loss of CO_2.

After formation of the growth nucleus growth proceeds as a first-order process.

Particle growth. There are two significant features of particle growth after formation of the growth nucleus. The first is the inflection in the growth curve and the second is the observed kinetics.

The shapes of the particles are also revealing. Considerations of simple geometry suggest that the initial oxide particles measured as plates, but with reaction there is a change in shape: the relative lengths of the axis changes toward what appears to be a more cubic shape. Electron microscopy suggests that the final product is a mixture of rectangular solids (*12*).

The inflections seem to mark the end of

one stage of growth and the beginning of a next. It is during this inflection that an apparent change in shape is occurring, and the last of the substantial disorder is lost. It is also about this inflection that a change in the rate law from first order to zero order occurs. However, the variance-range method shows that for one of the experiments (the observation of the CdO (220) plane at 649 K) the rate law on each side of the inflection is first order; the results for the other specimens are inconclusive. The results show that there is a change in the growth of the crystals, but that change is not the same for all planes.

An examination of the order of reaction and the rate constants in more detail remains. Notice that if Eq. (8) is linearized by expansion for small kt, it may be placed in the form of Eq. (10). The preexponential factors for growth during and after reaction are then seen to differ by two orders of magnitude. Thus the rate law is the same for the two periods of growth. The equality of the activation energies of the reaction period and the annealing period suggests that the mechanisms of growth are related, or perhaps the same, in both periods—the transition states are similar. It follows that the part of the mechanism observed cannot involve the formation and desorption of CO_2 directly, although the partial pressure of CO_2 may indeed effect the overall kinetics of the reaction (*18*). This is consistent with the differences in the Arrhenius form of the rate constant for mass loss, CdO appearance, and CdO particle growth.

A first-order process can be for a unimolecular reaction, hence the observed rate law for growth could involve CO_3^{2-} decomposition, but this is not likely, as discussed in the previous paragraph. A first-order process is also Avrami-type kinetics for the case $n = 1$, which is boundary saturation nucleation kinetics (*19*). Simple diffusion models also lead to first-order kinetics. A starting point for such a model is to envision that the oxide has a high degree of disorder after the CO_2 has formed and diffused from the solid. This oxide may have a low density. If the size of the oxide particles are proportional to the density of the crystallite ρ, then for the case with the boundary conditions for the region of reaction with diameter r_0,

$$\begin{aligned} \rho &= \rho^* \quad r = r_0, \qquad t \geq 0, \\ \rho &= \rho_0 \quad 0 < r < r_0, \quad t = 0, \end{aligned} \tag{12}$$

the diffusion equation yields

$$\alpha = 1 - \frac{6}{\pi^2} \sum_{n=0}^{\infty} \frac{\exp[-(n+1)D^*t]}{(n+1)^2}, \tag{13}$$

where α is the progress of the reaction at time t, and $D^* = \pi^2 D/r_0^2$, where D is the diffusion coefficient (*20*). Equation (13) may be truncated to give an approximate first-order process. The change in density in this model is brought about with the loss of CO_2 and subsequent rearrangement of ions near the interface of the oxide plates and the reaction region. The diffusion coefficient depends upon the mobility of the ions and the temperature. Notice that Eq. (13) may be linearized for small D^* to yield the rate law for postreaction growth.

After reaction is complete, the kinetics appears as that for Ostwald ripening for the case $n = 1$; it may indeed be of a different value of n, but the initial kinetics is masked by the reaction. The difference in the rate constants of the growth for the reaction and the postreaction periods is from the preexponential factor rather than the activation energy. To gain insight into the origin of the change in the preexponential factor, the diffusion coefficient found from the theory of absolute reaction rates may be considered (*21*):

$$D = \lambda^2 \frac{kT}{h} \frac{F^*}{F} \exp(-\varepsilon/kT), \tag{14}$$

where λ is the distance between successive equilibrium positions, F^* and F are the par-

tition functions in the activated and the normal state, and ε is the activation energy for an ion to jump between adjacent sites. For discussion, this can be simplified in the usual way. If the diffusion of ions is through a single vibrational mode, then there is one more vibrational degree of freedom in the activated state than in the normal state, and Eq. (14) is then

$$D = \lambda^2 \frac{kT}{h} \times [1 - \exp(-h\nu/kT)] \exp(-\varepsilon/kT), \quad (15)$$

where ν is the frequency of vibration for the diffusion path. If $h\nu/kT \ll 1$ this simplifies to

$$D = \lambda^2 \nu \exp(-\varepsilon/kT). \quad (16)$$

Thus, when the end of the reaction is reached, the frequency factor ν, and perhaps λ, may be altered, giving a lower preexponential factor. For the sintering region, the frequency of vibration of Eq. (16) is lower; this would arise from a change in the partition function when going from the phase where the CO_2 is being evolved to the final oxide product. A possible explanation for this change is that the former phase has a high concentration of defects. These defects would affect the partition function by making some vibrational, rotational, and translational modes more favorable for diffusion than for others of the final product; this in turn would affect the relative importance of the various mechanisms of diffusion. Any changes in the mechanism of diffusion would also change the form of the other preexponential terms as well as the partition functions in Eq. (14). Also, a decrease in the free energy of the CdO particles after reaction (from a decrease in porosity and defect concentration) would lower the rate constant (*19*).

The nonlinear behavior of the Arrhenius plot above 675 K may now be examined. Equation (15) cannot offer an explanation unless the partition functions are altered by the availability of more favorable vibrations and changes in the diffusion mechanisms. At temperatures above 700 K CdO sublimes, which would increase the number of defects and lower the activation energy as observed.

In addition, if the rate of annealing at this temperature is lower than that of CO_2 formation and diffusion, the result will be that the diffusion coefficient of the ions is anomalously larger than at lower temperatures by the formation of a more highly disordered phase. This disorder, by increasing the number of defects, would lower the activation energy so that the Arrhenius plot is nonlinear in this region. The growth characteristics of the reaction region extend beyond the end of the reaction as determined by the integrated intensities may be due not from sintering, but from the defect structure remaining from the rapid loss of CO_2. The growth and annealing from this disordered phase could account for the anomalous behavior.

The kinetics may be influenced by irradiation in three ways. The first is that the RPP may provide a second source of CdO; however, since the volume fraction of this phase is relatively small the kinetics should not be adversely affected. Second, radiation may initiate nucleation or create additional nucleation sites. Third, it may increase growth at a reaction interface where there is substantial strain. The rates of mass loss, CdO appearance, and CdO growth are comparable even though the Arrhenius form of the rate constants are not; indeed, if there are any differences in the rates, it is the rate of mass loss that is the greatest. Although a radiation affect cannot be discounted, and more work is required, it is seen not to have a strong impact on the observed kinetics.

Conclusion

The TRXD of the thermal decomposition of $CdCO_3$ and $Cd(OH)_2$ powders show that time resolved X-ray diffraction is a useful

technique to study solid-state reactions. The change in shape of the diffraction lines may be followed as the reaction proceeds and then as sintering and annealing of the product occurs. The observed line shapes are indeed related to the reaction, and valuable information can be extracted by the analysis of these shapes. For TRXD, a complete size and strain analysis of the diffraction lines is possible, and for these experiments a greater understanding of solid-state decomposition reactions is obtained.

In brief, for the formation of CdO from the decomposition of $CdCO_3$, the growth proceeds from an initial particle ~60 Å in diameter. The particle growth during reaction is first order and during sintering is zero order. The rate constants differ only by the preexponential factor. A high degree of disorder is observed during reaction, and the final product has low strain. The growth displays a transition from the kinetics of particle growth during reaction to that during sintering. At ~700 K, the rate constants become lower than what is expected from a linear Arrhenius plot.

Acknowledgments

The funds for this work were provided by the National Science Foundation. We also thank Dr. Yow Lin and Hong Ma for their assistance in data collection and the staff of SSRL for their help.

References

1. T. L. Groy, S. H. Lin, S. K. Porter, R. R. Von Dreele, and L. Eyring, *J. Mol. Sci.* **2,** 93 (1982).
2. O. Savborg, J. R. Schoonover, S. H. Lin, and L. Eyring, *J. Solid State Chem.* **68,** 214 (1987).
3. J. Green, *J. Mater. Sci.* **18,** 637 (1983).
4. G. Brauer, Ed., "Handbook of Preparative Inorganic Chemistry," 2nd ed., Academic Press, New York (1965).
5. A. J. C. Wilson, "X-Ray Optics," Methuen, London (1962).
6. J. I. Langford, *J. Appl. Crystallogr.* **15,** 315 (1982).
7. G. B. Mitra, *Acta Crystallogr.* **17,** 765 (1964).
8. J. I. Langford and A. J. C. Wilson, "Crystallography and Crystal Perfection," p. 207. Academic Press, New York (1963).
9. R. Sh. Mikhail, D. Dollimore, A. M. Kamel, and N. R. El-Nazer, *J. Appl. Chem. Biotechnol.* **23,** 419 (1973).
10. B. J. Asirvatham and Z. A. Munir, *J. Mater. Sci.* **21,** 1997 (1986).
11. J. B. Hastings, W. Thomlinson, and D. E. Cox, *J. Appl. Crystallogr.* **17,** 85 (1984).
12. Z. A. Munir and B. J. Asirvatham, *J. Mater. Sci.* **21,** 2002 (1986).
13. R. Sh. Mikhail, D. Dollimore, A. M. Kamel, and N. R. El-Nazer, *J. Appl. Chem. Biotechnol.* **23,** 431 (1973).
14. J. R. Schoonover, PhD. Dissertation, Arizona State University (1988).
15. R. C. Garvie, "High Temperature Oxides" (A. M. Alper, Ed.), Vol. 2. Academic Press, New York (1970).
16. B. E. Warren, "X-ray Diffraction," Addison, New York (1969).
17. E. A. Prodap and M. M. Poulyuchenko, *Geterog. Khim. Reakts.* **50,** 79 (1961).
18. Z. A. Munir and J. L. Rice, *High Temp. Sci.* **14,** 171 (1981).
19. J. W. Christian, "The Theory of Phase Transformation in Metals and Alloys," Part I, 2nd ed., Pergamon Press, New York (1975).
20. H. Eyring, S. H. Lin, and S. M. Lin, "Basic Chemical Kinetics," Wiley–Interscience, New York (1980).
21. S. Glasstone, K. J. Laidler, and H. Eyring, "The Theory of Rate Processes," McGraw–Hill, New York (1941).